Polymer 246 (2022) 124723

Contents lists available at ScienceDirect

Polymer

journal homepage: www.elsevier.com/locate/polymer

Solvent-structured PEDOT:PSS surfaces: Fabrication strategies and nanoscale properties

Matteo Sanviti [a,b], Lars Mester [c], Rainer Hillenbrand [d,e], Angel Alegría [a,b,*], Daniel E. Martínez-Tong [a,b,**]

[a] Centro de Física de Materiales (CFM, CSIC-UPV/EHU). P. Manuel Lardizábal 5, 20018, San Sebastián, Spain
[b] Departamento Polímeros y Materiales Avanzados: Física, Química y Tecnología, University of the Basque Country (UPV/EHU). P. Manuel Lardizábal 3, 20018, San Sebastián, Spain
[c] CIC NanoGUNE BRTA, 20018, Donostia-San Sebastián, Spain
[d] CIC NanoGUNE BRTA and Department of Electricity and Electronics, EHU/UPV, 20018, Donostia-San Sebastián, Spain
[e] IKERBASQUE, Basque Foundation for Science, 48011, Bilbao, Spain

ARTICLE INFO

Keywords:
AFM-nanostructure
Conductivity
Polymer materials

ABSTRACT

We present the preparation of nanostructured conducting PEDOT:PSS thin films by solvent vapor annealing (SVA), using the low boiling point solvent tetrahydrofuran (THF). An Atomic Force Microscopy (AFM) study allowed the observation of distinct nanostructure development as a function of solvent exposure time. Moreover, the nanostructures' physical properties were evaluated by nanomechanical, nanoelectrical, and nanoinfrared (nano-FTIR) measurements. In this way, we were able to differentiate the local response of the developed phases and to identify their chemical nature. The combination of these techniques allowed to demonstrate that exposure to THF is a facile method to effectively and selectively modify the surface nanostructure of PEDOT:PSS, and thereafter its final properties. Moreover, our nanoscale studies provided evidence about the molecular rearrangements that PEDOT:PSS suffers during nanostructure fabrication, a fundamental fact in order to expand the potential applications of this polymer in thermoelectric and optoelectronic devices.

1. Introduction

Nowadays, poly(3,4-ethylenedioxythiophene):poly(styrenesulfonate) (PEDOT:PSS) is one of the most employed intrinsically conducting polymers on the industrial market [1]. Its success is related to its unique optoelectronic properties [2], high and tunable electrical [3,4] and thermoelectrical properties [5–9], and excellent physicochemical stability [10]. In this way, PEDOT:PSS has been used in applications as low consuming organic light-emitting diodes [11,12] and highly effective perovskite solar cells [13,14], which are being highly demanded for developing a more sustainable and greener future.

The PEDOT:PSS nanostructure and morphology – especially at the surface – has captured important attention in recent years [15]. In this regard, two main approaches have been explored to tune and enhance the resulting PEDOT:PSS properties and physical behavior. On one hand, several authors have focused on modifying the PEDOT:PSS surface properties, as its work function and electrical/thermoelectrical response, while leaving mostly unchanged its surface morphology. For example, the removal of the free PSS phase that connects the PEDOT:PSS rich grains in the thin film geometry allowed to increase the thin film electrical conductivity [16–18], without important impact to the surface topography. For this purpose, many solvent-based methods have been largely used, mostly employing high boiling point polar molecules as ethylene glycol (EG), dimethyl sulfoxide (DMSO), or dimethylformamide (DMF), as well as other liquids as alcohols, sorbitol and acids [16,19]. Also, the use of other molecules has allowed to tune the polymer's work function [20–23]. In particular, using tetrakis(dimethylamino) ethylene (TDAE), it was possible to reduce superficial PEDOT from its polaron/bipolaron state ($PEDOT^{+/2+}$) to the neutral state ($PEDOT^{0}$), while preserving its good electrical conductivity [20].

On the other hand, the fabrication of precise PEDOT:PSS nanostructures have permitted the modification and enhancement of the resulting polymer properties [24–27], in turn, leading to boosted applications [28–34]. In this way, several groups have developed different

* Corresponding author. Centro de Física de Materiales (CFM, CSIC-UPV/EHU). P. Manuel Lardizábal 5, 20018, San Sebastián, Spain.
** Corresponding author. Centro de Física de Materiales (CFM, CSIC-UPV/EHU). P. Manuel Lardizábal 5, 20018, San Sebastián, Spain.
E-mail addresses: angel.alegria@ehu.eus (A. Alegría), danielenrique.martinezt@ehu.eus (D.E. Martínez-Tong).

https://doi.org/10.1016/j.polymer.2022.124723
Received 16 November 2021; Received in revised form 20 February 2022; Accepted 4 March 2022
Available online 11 March 2022

nanostructured PEDOT:PSS surfaces by laser irradiation [27,31,33,35,36], nanoimprint lithography [25,29,37,38], and by using templates and molds [31,34,39]. In these works, it was possible to fabricate distinct surface features as linear nanostructures or nanogratings [25,27,34,35,37,39], nanocavities [36], nanopores/nanopillars [31], hemispherical patterns [29], with characteristics lengths ranging from 10^2-10^4 nm. For example, very recently Gutiérrez-Fernández and collaborators presented an ablation-free method to prepare nanostructured PEDOT:PSS surfaces by laser irradiation [27]. In their work, the authors managed to create nanogratings, with a characteristic period of ~250 nm, without inducing strong modifications to the physical properties of the polymer. In particular, the authors found a partial segregation of the conducting domains towards the lower phases of the gratings, allowing preparing functional nanostructures. However, in counterpart, most of the so-far presented methods for nanostructuring PEDOT:PSS are highly demanding since they require special facilities, or might risk the physicochemical stability of PEDOT:PSS. For example, nanoimprint lithography on PEDOT:PSS can be difficult to perform due to the non-thermoplastic property of this material [40]. Also, it requires access to clean room facilities and the use of a nanopatterned stamp, introducing several conditions to fulfill prior the actual nanostructuring process. Moreover, the use of laser-based PEDOT:PSS nanostructuring has been mostly applied by ablating the polymer surface [33,35,36,41]. By this high energy process, the polymer material is prone to suffer physicochemical modifications that might alter its resulting behavior.

In our work, we present the fabrication of surface nanostructures on PEDOT:PSS thin films by exposing the polymer to tetrahydrofuran (THF) solvent vapors. Our solvent treatments resulted in drastic changes of the PEDOT:PSS surface morphology, allowing the fabrication of custom structures based on solvent exposure time. We evaluated the mechanical and conductive properties of the nanostructured polymer by different nanoscale measurements, including nanomechanical atomic force microscopy (AFM), conductive AFM, and nanoscale Fourier transform infrared (nano-FTIR) spectroscopy. In this way, we determined the impact of nanostructure formation on PEDOT/PSS morphology and phase segregation, as well as the conductivity, Young's modulus, and chemical composition of the samples. In particular, we found an enriched sheet of neutral state PEDOT species ($PEDOT^0$) at the upmost layer of the solvent-structured thin films. Our methodology provides a new and facile method to effectively and selectively modify the surface nanostructure of PEDOT:PSS and thereafter its final properties, to expand its potential applications in thermoelectric and optoelectronic devices.

2. Experimental section

2.1. Materials

Poly(3,4-ethylenedioxythiophene):polystyrene sulfonate (PEDOT:PSS) was purchased from Sigma-Aldrich (product #655201, water dispersion 3–4 wt%). The polymer was used as received. Tetrahydrofuran (THF) was purchased from Scharlab (product TE02282500).

2.2. Thin films preparation

Thin films of pristine PEDOT:PSS and PSS were cast onto Indium Tin Oxide (ITO) substrates (Ossila, product #S111) by spin coating, at 3000 rpm for 2 min (usual ITO substrate size was 10 × 5 mm). Prior spin coating, the ITO substrates were washed in acetone and dried under a nitrogen flow. After spin coating, the thin films were transferred to a high vacuum chamber (pressure $<10^{-5}$ bar) and left overnight (~16 h) at room temperature to allow the evaporation of remaining water molecules.

2.3. Nanostructure fabrication

For the fabrication of solvent-structured PEDOT:PSS surfaces we explored two strategies. First, for fast solvent exposure, we spin casted a drop of THF onto the PEDOT:PSS thin films. Here, a drop of solvent coated the whole material surface, forming a meniscus, and spinning started immediately afterwards. Second, for long solvent exposure, we carried out solvent vapor annealing (SVA) treatments, following a previously reported procedure [42]. For SVA, we used a glass desiccator (inner diameter = 150 mm) saturated with THF vapors. This chamber was prepared by leaving a pure volume of THF (20 mL), free to evaporate inside it. The solvent was replaced as many times as required until it preserved its volume without further evaporation. The polymer pristine thin films were subjected to solvent vapors for different times. For both strategies, after solvent exposure, the films were left again in high vacuum, overnight and at room temperature, to allow evaporation of possible residual solvent.

2.4. Methods

Atomic Force Microscopy (AFM) measurements were acquired at room conditions (50% RH, 24 °C), using a Multimode microscope, and Nanoscope V electronics (Bruker). The system was controlled by the Nanoscope 8.15 software (Build R3Sr8.103795). All AFM images and maps were analyzed using Nanoscope 1.90 (Bruker).

Topography characterization of the samples was performed using the PeakForce Tapping mode, and Tap300Al-G probes (BudgetSensors). From the topography images, the mean surface roughness (R_a) was calculated as $R_a = N^{-1}\sum_{i=1}^{N}|z_i - z_0|$, where N is the total number of pixels in the image, $|z_i - z_0|$ the average height value at the i-th pixel of the image, from the mean plane (z_0).

The nanoelectrical properties of the PEDOT:PSS thin films were measured by the conductive-AFM (C-AFM) method, using the so-called TUNA protocol with the same AFM equipment. C-AFM method allows the evaluation of the samples' conductivity by measuring the current flowing through the material [43]. For this purpose, the PEDOT:PSS thin films on ITO substrates were electrically connected to the metallic sample holder using silver paint (RS components, product #189–3593). For C-AFM measurements, we used diamond-coated conductive probes (DDESP-FM-10, Bruker). Electrical current maps were obtained by applying DC bias (10 mV) to the sample stage (S_{BIAS}) while scanning. The current flowing through the sample was detected via the probe using a current amplifier (Extended TUNA, Bruker), at a 1 nA/V sensitivity. Prior the experiments, the diamond-coated probes were calibrated to allow a precise force control, as follows. The cantilevers' spring constant was determined by Sader's method [44,45] resulting in usual values of about 5 N/m. The photodetector sensitivity was calibrated using a force-distance curve against a sapphire standard (Bruker), leading to usual values of ~50 nm/V. In this way, for all the C-AFM imaging experiments, we used a fixed probe deflection setpoint of 2.5 nm, which was equivalent to ~12.5 nN of probe-sample normal force. This allowed testing the electrical properties without compromising the material's topography and the probe quality. Based on the electrical current maps, on selected areas of the surface we performed current-voltage characteristics (I–V curves). For this process, a DC voltage ramp was applied to the sample in the $-10\ mV \leq S_{BIAS} \leq 10\ mV$ range, at a 1 Hz rate and collecting about 9000 points. For this purpose, we increased the probe-sample normal force to 75 nN to ensure a good probe-sample electrical contact. The data obtained from the I–V curves was analyzed in conformity following previous reported methods [46,47].

Nanomechanical studies were conducted using the PeakForce-QNM method (PF-QNM), using Tap300Al-G probes. For PF-QNM measurements the system was calibrated following recent literature reports

[48–50]. Briefly, the cantilevers' spring constant was calculated using Sader's method, resulting in typical values of 20 N/m. The photodetector sensitivity was calibrated by performing a linear force-distance curve against a sapphire standard (1 Hz, *Z*-ramp = 200 nm, trigger threshold = 0.2 V). The deflection sensitivity was verified during PF-QNM operation, using the same sapphire sample (PeakForce frequency = 2 kHz, PeakForce amplitude = 100 nm, PeakForce setpoint = 0.2 V), allowing a maximum 10% deviation between the PF-QNM and force-distance results. Immediately afterwards, the "Sync Distance" parameter was evaluated using the sapphire sample. This parameter is a time constant at which the Z piezo is at its lowest travelling position during PF-QNM imaging, and it is fundamental in order to obtain quantitative values [51,52]. The obtained value was fixed during all PF-QNM measurements performed on the PEDOT:PSS thin films. Finally, the tip end-radius was obtained by the evaluation of a force-distance curve on a polystyrene thin film, with a nominal Young's modulus (E_Y) of 3 GPa. Typical end-radii were in the 10–12 nm range. In all cases, PF-QNM measurements were carried out using a PeakForce setpoint value of 20 nN. From PF-QNM data, we calculated Young's modulus maps, using the simplified Derjaguin-Müller-Toporov (DMT) approximation as [53,54]:

$$F - F_{adh} = \frac{4}{3}\frac{E_Y}{(1-\nu^2)}\sqrt{R}\delta^{3/2} \quad (1)$$

where F is the applied force, F_{adh} the probe-sample adhesion force, ν the Poisson ratio, R_{tip} the tip end-radius, δ the probe-sample indentation, and E_Y the Young's modulus. Eqn (1) was fitted to the PF-QNM dynamic force-distance retrace curves, in the 30–90% range of total force (see Supplementary Information).

Nano-FTIR spectroscopy [55–57] is based on Fourier transform infrared spectroscopy of light scattered from a metallic AFM tip. It allows for nanoscale chemical characterization of a wide range of organic and inorganic sample systems and material properties such as infrared absorption [55] or carrier concentrations [56,58]. Here we used a commercial nano-FTIR setup (neaSNOM by neaspec GmbH) with two integrated broadband laser light sources (covering the mid-IR and near-IR spectral ranges; respectively 700–1700 cm^{-1} and 2600–3600 cm^{-1}) in combination with standard PtIr-coated AFM tips (Arrow NCPt, Nanoworld, tip radius 30 nm), yielding a spatial resolution of about 30 nm independent on the wavelength. The infrared radiation is focused onto the AFM tip that acts as optical antenna [59], effectively focusing the infrared radiation into a concentrated electromagnetic hot spot below the tip apex. Near-field interaction between the tip and sample modifies the tip-scattered light, the latter being detected by an assymmetric Fourier transform spectrometer (based on a Michelson interferometer) including a MCT detector. In contrast to far-field FTIR spectroscopy, the sample and the tip are located in one of the arms of the interferometer, yielding amplitude- and phase-resolved infrared spectra. Unwanted background signals are suppressed by operating the AFM in tapping mode (tip oscillation amplitude 50 nm and frequency 250 kHz) and demodulating the detector signal at the 3rd higher harmonic of the tip oscillation frequency [55,57]. In this work, we show amplitude spectra, which can be interpreted (qualitatively) as local infrared near-field reflection spectra.

Calculated nano-FTIR spectra were obtained using the finite dipole model (FDM) for semi-infinite samples [60]. In the model, the AFM tip is approximated as a prolate spheroid with a major half-axis length 300 nm and apex radius 30 nm, that is oscillating sinusoidally above the sample surface with a tapping amplitude of 50 nm (corresponding to the experimental values). The near-fields created by a point charge near the tip apex are (quasi-)electrostatically reflected at the sample surface and induce an additional charge distribution in the tip. The model parameter $g = 0.7e^{0.06i}$ describes which part of the induced charge is effectively relevant for the near-field interaction [60]. nano-FTIR amplitude spectra are described in the model by the absolute value of the effective polarizability $\alpha_{eff} = 0.5(\beta f_0)/(1\text{-}\beta f_1)$ of the coupled tip-sample system, where f_0 and f_1 are geometry factors [60] and β is the sample's electrostatic reflection coefficient that for semi-infinite samples depends solely on the sample's permittivity ε, i.e. $\beta = (\varepsilon\text{-}1)/(\varepsilon+1)$. For layered samples we use modified expressions given in Ref. [61].

3. Results & discussion

3.1. Nanostructure formation by exposure to THF

Fig. 1(a and b) show the surface topography of a PEDOT:PSS thin film, obtained from the commercial PEDOT:PSS water dispersion, without any further treatment (pristine sample). We observed a continuous surface with a mean roughness of 3.4 nm, comprised by granules with a mean diameter of ~50 nm (Fig. 1b). These surface features were in line with those previously reported for PEDOT:PSS thin films [62–65], where dried PEDOT:PSS has been reported as composed by highly conducting PEDOT:PSS grains, each coated with a thin shell of PSS [65,66]. We evaluated the PEDOT:PSS thin film thickness via AFM, by scratching the surface using sharp tweezers and measuring height between the sample/substrate step. This analysis allowed obtaining a thickness value ~400 nm for this sample. All the determined structural features for the PEDOT:PSS sample are summarized in Table 1.

Fig. 1(c–f) show the surface structure of PEDOT:PSS after two different THF treatments, *i.e.*, *short* and *long* solvent exposure times (t_e). Samples nanostructured by a short exposure to THF ($t_e \ll 1$ min), were prepared by spin casting a drop of THF onto pristine PEDOT:PSS thin films (see Experimental Section). We found that the surface topography was affected by the fast interaction with the solvent, as shown in Fig. 1(c and d). In this sample, from now on called PEDOT:PSS-ST, we observed the formation of randomly distributed holes on the PEDOT:PSS surface. These inclusions had a typical diameter of ~250 nm, and depths of ~18 nm. No changes in the film thickness were detected and the overall film's roughness ($< R_a >$) was about 3.0 nm. Moreover, by taking a closer look to the AFM topography images, we observed that the PEDOT:PSS granular structure could not be distinguished anymore on the highest areas of the surface (see green arrows in Fig. 1c). This observation can be further appreciated by comparing Fig. 1b and d and their respective cross-sections. We confirmed the observations by calculating the roughness of the upmost layer (R_{a-up}) of PEDOT:PSS-ST, which resulted in typical values of ~1.0 nm, *i.e.*, ~70% lower when compared to the pristine PEDOT:PSS sample (Table 1).

Although a fast exposure of PEDOT:PSS thin films to THF resulted in a nanostructured surface, we must highlight two observations that hinder its application as structuring strategy. First, the observed changes were not homogeneous throughout the whole film surface, since different areas of the material presented different features as shown in Fig. S1 (Supplementary Information). This fact can be related to an inhomogeneous distribution of the solvent on the polymer surface during spinning. Second, the resulting structures changed dramatically only by small variations the spin coating process. For example, fairly different structures were obtained if the THF drop was casted once the spinning began or, on the opposite way, by waiting a couple of seconds between casting the solvent and starting the spinning (Fig. S2). These set of observations were fundamental towards the use of spin casting for the modification of PEDOT:PSS thin films in a reproducible manner.

Comparing our results with previous works, we found that there are several reports dealing with the use of different solvents to tailor and tune PEDOT:PSS properties [67–69]. In most cases, the works have used high boiling point solvents, as EG Refs. [13,68,70], DMF [70] and DMSO [67–70], or alcohols as ethanol or methanol [13,71]. In these reports, the authors did not observed the formation of well-defined nanostructures, as the ones obtained in our current work using THF. However, most authors reported some changes in the surface roughness that, in some cases, allowed a better adhesion of further layers during final device fabrication [67]. Moreover, these high boiling points solvents

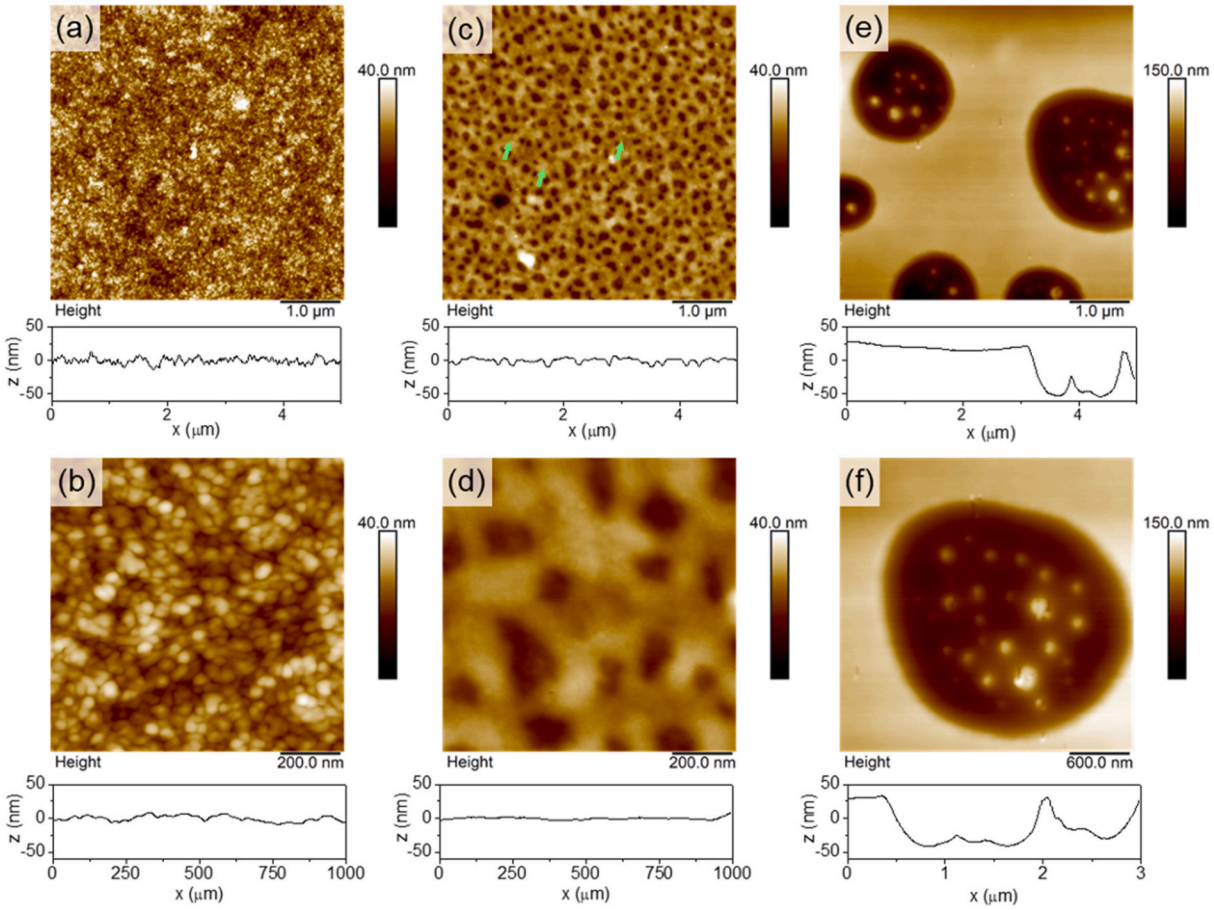

Fig. 1. AFM topography images of PEDOT:PSS thin films treated with THF: (a,b) pristine sample, (c,d) after short interaction times ($t_e \ll 1$min), and (e,f) after long interaction times ($t_e = 10$ min). A topography cross-section, taken at the center of each image, is presented below each figure.

Table 1
PEDOT:PSS structural features, as determined by AFM measurements. In this table, t is the exposure time, h the film thickness, $< R_a >$ the overall roughness (whole film), R_{a-up} the roughness of the upmost layer, h_D the depth of the inclusions, and D_I the diameter of the inclusions.

Sample	t_e	h	$< R_a >$	R_{a-up}	h_D	D_i
Pristine	–	400 ± 10 nm	3.4 ± 0.2 nm	–	–	–
PEDOT:PSS-ST	≪1 min		3.0 ± 0.2 nm	1.0 ± 0.2 nm	18 ± 2 nm	220 ± 50 nm
PEDOT:PSS-LT	10 min		23 ± 1 nm	0.5 ± 0.2 nm	30 ± 10 nm	0.8–3 μm

allowed tuning the PEDOT:PSS electrical properties, in most cases enhancing the electrical conductivity of the polymer. Nonetheless, an improved electrical conductivity is not the unique factor to consider when tailoring PEDOT:PSS for final applications [70,72,73]. For example, Liu et al. were able increase the transport properties of PEDOT:PSS thin films by spin casting EG, DMF, and/or DMSO [70]. However, the authors observed that the treated films, with enhanced conductivities, led to poorer device performance in perovskite-based solar cells. In fact, in their work, the authors determined that by inserting a thin layer of non-conducting PSS between the PEDOT:PSS and the perovskite films allowed improving the final device behavior, since PSS allowed a better perovskite adhesion and film formation [70,72]. In our work, exposure of the PEDOT:PSS thin film to THF vapors also allowed its controlled nanostructuring, as presented in the following lines.

Fig. 1(e and f) show the topography of a PEDOT:PSS thin film after a long exposure to a saturated THF atmosphere ($t_e = 10$ min). We will refer to this sample as PEDOT:PSS-LT from now on. Here, the sample was subjected to an SVA treatment that allowed a good control of exposure time (see Experimental section). As shown by the AFM topography images, the long exposure to THF vapors resulted in a further surface nanostructuring, compared to PEDOT:PSS-ST. Now, the PEDOT:PSS surface was characterized by clearly defined micrometer-sized domains, as if the holes observed for short times kept on increasing due to the influence of the THF vapors. The domain depth was about 40 nm (× 2 deeper), while their diameter ranged between 0.8 and 3 μm (up to × 10 larger, compared to PEDOT:PSS-ST). The characterization of different samples of PEDOT:PSS-LT, revealed that the domains not always show a regular circular geometry and they present a typical depth of 30 ± 10 nm. Inside these features, there were other nanometric structures, as islands with typical diameters of 250 nm, and varying heights (Fig. 1f). No changes in the film thickness were detected, as measured from the upper layer, indicating that long exposure to THF vapors did not result in film dewetting. Finally, the upmost layer of this sample presented again an extremely low roughness value ($R_{a-up} = 0.5$ nm), even lower to those found for the flat areas of PEDOT:PSS-ST.

Furthermore, we explored how SVA exposure at different times allowed to prepare different nanostructures on the PEDOT:PSS surface. When using $t_e < 10$ min, a similar problem to that found for spin casting was observed: although surface nanostructuring was possible, the formed features were not reproducible. For example, Figs. S3(a and b) show two PEDOT:PSS thin film treated by SVA for 7 min where particularly different features were formed. In the specific case of Fig. S3b, we observed the initial formation of the inclusions in PEDOT:PSS, characterized by lower values of depth, diameter and $< R_a >$. For longer treatment times, $t_e \geq 10$ min, homogeneous surface nanostructuring

was achieved. However, for exposure times of 30 and 60 min, the $< R_a >$ increased dramatically to values ranging from 30 to 70 nm. In these two cases, AFM images (Figs. S3(c–f)) showed the breakage of the upper part of the PEDOT:PSS thin film, forming now aggregates of 50–300 nm in diameter and ~40 nm of height, for a 30 min treatment. Interestingly enough, after 60 min of solvent exposure these aggregates reached an almost homogeneous size distribution, with diameters and height of 150 nm and 40 nm, respectively. Moreover, for these two cases we observed spherulites in random areas of the films, covering micrometer sized areas of about 4 μm in diameter, and 200 nm of height. Finally, it is worth highlighting that the observed structural rearrangement did not result in film dewetting, but in a thickness reduction. In particular, we were able to quantify a film thickness of ~300 nm for 30 and 60 min SVA treated films, as measured from the homogeneous surface outside the crystalline domains down to the supporting ITO substrate.

Previously, different SVA strategies were used to modify and enhance the behavior of PEDOT:PSS thin films [3,74–78]. In most cases, the reported works have focused on tailoring the electric and thermoelectric properties of PEDOT:PSS using DMSO vapors [3,74–77]. However, only a few reports have focused on the SVA impact on surface topography and nanostructure formation, where most investigations have pointed out the separation of PEDOT from PSS after solvent exposure. For example, Xu and collaborators observed the formation of smooth and uniform film morphologies after exposing PEDOT:PSS thin films to DMSO vapors for up to 60 min [3]. The authors associated this structure to the fusion of the PEDOT:PSS grains, which in turn reduced the tunneling distance between molecules and led to enhanced conductivities. Also, Yeo et al. [69,75] showed that SVA of PEDOT:PSS thin films, using DMSO for up to 120 min, resulted in an homogeneous surface topography with a fairly low roughness of 0.38 nm. This value was comparable to the R_{a-up} calculated for PEDOT:PSS-LT in our present study (0.5 nm). In their work, the authors associated this topography to the formation of an enriched-PSS layer on the top surface of the SVA-treated films, *i.e.*, a vertical PEDOT/PSS phase separation took place due to solvent exposure. This PSS segregation towards the surface allowed preparing PEDOT:PSS anode films with enhanced conductivities and tunable work functions [69]. However, none of these research works have shown the possibility of using a SVA strategy to efficiently nanostructure PEDOT:PSS samples, as in our present study. Then, in order to understand the nature of the different structural phases of the PEDOT:PSS-LT sample, we have investigated its physical properties.

3.2. Transport properties of nanostructured PEDOT:PSS thin films

Fig. 2 shows the nanoscale electrical transport properties of PEDOT:PSS-LT. In particular, Fig. 2a shows the topography of the sample, as obtained from TUNA experiments. We observed that the scanning process did not result in damage to the surface, under the applied normal force conditions. Fig. 2b presents the electrical current map (TUNA current), in a binary color scheme. There, green areas denote electrically conducting areas, while black areas show *non-conducting* areas of the sample. For this binary approach, we selected a current cutoff of 100 pA. This idea allowed highlighting those areas which electrical current values were comparable to those reported for pristine PEDOT:PSS [79]. We observed that the electrical current map of PEDOT:PSS-LT was heterogeneous, *i.e.*, only some parts of the sample presented an electrical current flow directly ascribable to the pristine material. In other words, solvent exposure resulted in a segregation of conducting domains. As shown in Fig. 2b, the electrical conducting regions were composed by a collection of conducting spots, in line with previous reports for PEDOT:PSS thin films [26,46,80,81]. To link the relations between the formation of surface nanostructures and segregation of conducting domains, in

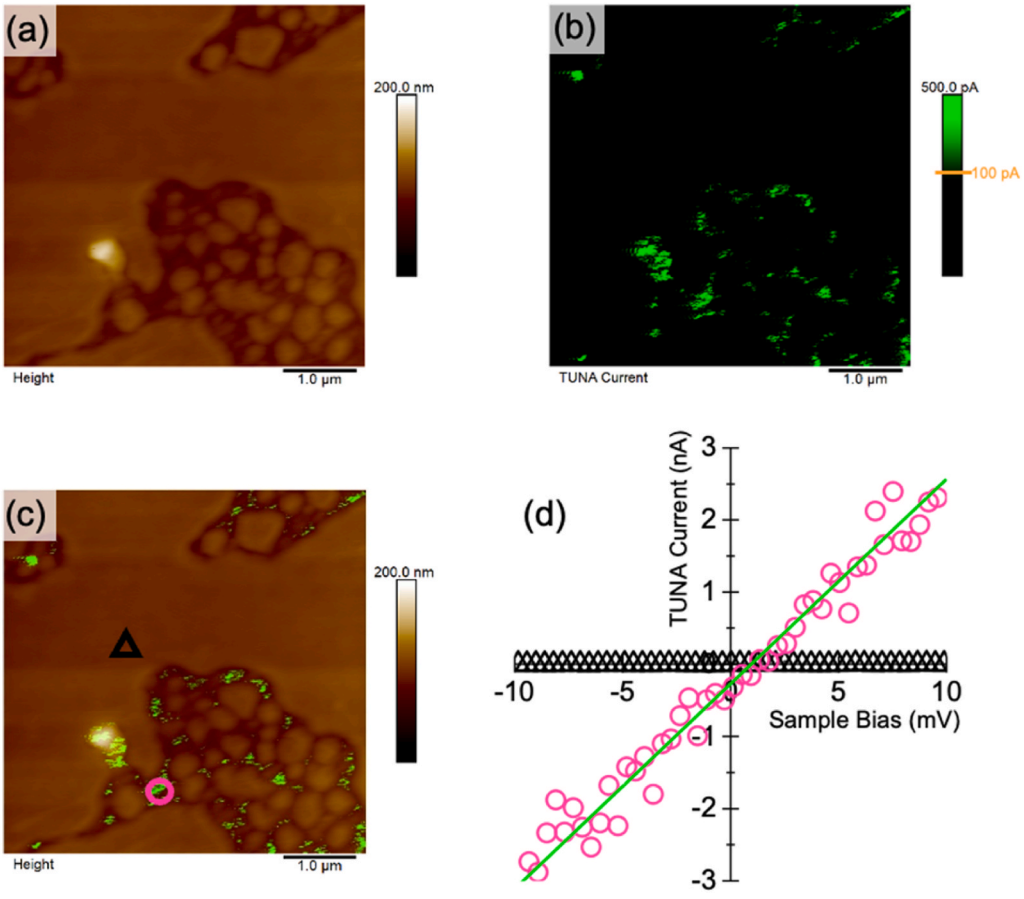

Fig. 2. Nanoelectrical properties of PEDOT:PSS-LT, as determined by TUNA experiments. (a) Topography. (b) Electrical current map. Green areas indicate electrical current values above 100 pA. (c) Compound topography/current image. Green shading denotes regions of the sample with current values higher than 100 pA. (d) Current-voltage characteristics (I–V curves) performed by TUNA experiments on two spots of the PEDOT:PSS-LT sample (see triangle and circle in Fig. 2c). Green continuous line in Fig. 2d is a linear fit to the data (circles only). The data shown for Fig. 2d are presented as 1 point each 200 captured datapoints. (For interpretation of the references to color in this figure legend, the reader is referred to the Web version of this article.)

Fig. 2c we present a compound *topography/electrical* map. Here, the green shading over the topography image indicates those areas showing electrical current above 100 pA. By this approach, we were able to determine that the bottom phases of the PEDOT:PSS-LT sample were the only ones showing electrical current flow comparable to pristine PEDOT:PSS. On the contrary, both the upper phase and the spherical islands presented current values well below our cutoff limit, indicating that these zones did not allow electronic transport under our evaluation conditions. Using the TUNA current maps, we were able to calculate a typical conductance of ~0.5 nS. This value was on the same order of magnitude to those found previously for PEDOT:PSS using C-AFM electrical mapping [27,81].

In order to provide a precise measure of the conductivity of the different phases composing the PEDOT:PSS-LT sample, we performed I–V measurements at the distinct regions. Fig. 2d shows the obtained results at two representative spots of the samples, as marked in Fig. 2c. The top phase of PEDOT:PSS-LT showed a response characteristic of a dielectric material, as observed from the black triangles in Fig. 2d. Even by increasing the sample bias and evaluating the current flow with the highest amplification possible (10 pA/mV), the detection was still zero. On the contrary, at the bottom phase, a linear I–V relationship was found (open circles in Fig. 2d). By fitting the data to a linear function (green line in Fig. 2d), from the slope value a conductance (G) of 0.284 ± 0.001 nA/mV was obtained. Using this value, a resistance (R) of 3.52 ± 0.01 MΩ was calculated. Then, we were able to calculate the conductivity of the material (σ) as:

$$\sigma = \frac{h}{R \cdot s} \tag{2}$$

where s is the tip-sample contact area, calculated as 3.5×10^{-16} m^2 (see Supplementary Information), and h is the phase thickness. Following eqn. (2), we obtained a conductivity of 3.1 ± 0. 1 S/cm for the bottom phase of PEDOT:PSS-LT. For direct comparison, we measured an I–V curve on a pristine PEDOT:PSS thin film, with the same instrumental setup (Fig. S4). Again, a linear I–V relation was obtained, from which a conductivity of 2.5 ± 0.1 S/cm was calculated. This result evidenced that the bottom phase of PEDOT:PSS-LT preserved the good electronic transport properties of the pristine polymer. Please beware that the obtained conductivity values correspond to an out-of-plane charge transport process, *i.e.*, a current flowing from the ITO substrate to the AFM tip, throughout the whole volume of the PEDOT:PSS thin film. Our obtained conductivity results are about 5–10 times higher than those reported previously for PEDOT:PSS thin films, using also C-AFM methods [46,81]. However, these differences can be understand by the different physicochemical nature of PEDOT:PSS samples used in these studies. For example, changes in the polymer molecular weight, PEDOT/PSS ratios, and film thickness lead to changes in the overall transport properties of this material, as previously reported [66,82].

Further nanoelectrical experiments allowed to evaluate the disposition of the upper PEDOT:PSS-LT phase and its penetration onto the thin film volume. In this case, we detected the variation of the conductivity along the film thickness by using a controlled penetration of the AFM tip into the sample, as summarized in Fig. 3.

Going into detail, on an arbitrary spot on the upper layer of the PEDOT:PSS-LT sample, indicated by the red circle in Fig. 3a, we measured an I–V curve at the usual conditions. At this initial point, the corresponding I–V spectra showed the non-conducting behavior of the upper phase just discussed. We progressively increased the force set-point between the tip and the surface, acquiring an I–V curve at every step. When the normal force was increased above ~300 nN, an ohmic

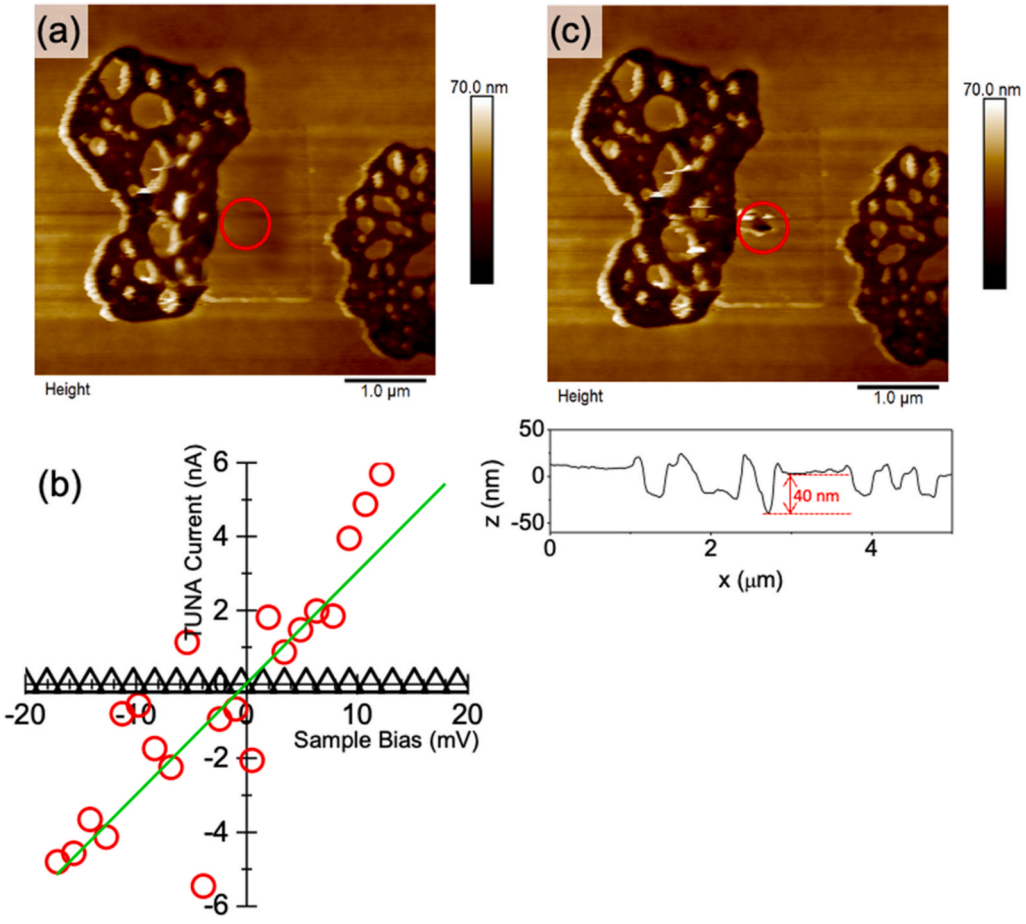

Fig. 3. (a) AFM topography image of a selected PEDOT:PSS-LT area. (b) I–V curves on the PEDOT:PSS-LT sample before (triangle) and after (circles) nanoindentation. In both cases, data is shown as 1 every 20 points. Green line shows a linear fit to the circles. (c) AFM topography image of the same PEDOT:PSS-LT area after nanoindentation. Below the image, a height cross-section is presented, taken at the center of the print left by nanoindentation. (For interpretation of the references to color in this figure legend, the reader is referred to the Web version of this article.)

I–V curve was obtained, with a resistance of = 2.3 MΩ (Fig. 3b), indicating that we penetrated the surface deep enough to reach a conductive path. The obtained resistance was fairly similar to that of the bottom phase of PEDOT:PSS-LT, previously presented. After this experiment, a topography image was taken to evaluate the indentation depth necessary to reach the conductive material (Fig. 3c). We found that the imprint left after the indentation experiment had a depth of 40 nm; a value comparable to the average thickness of the upper phase (see vertical cross-section in Fig. 3c). Our nanoindentantion results thus confirmed that the PEDOT:PSS-LT upper phase did not reach the bottom of the film, but formed only a *covering sheet* of a few nanometers thick, leaving a PEDOT:PSS volume below it. In other words, the bulk properties of the PEDOT:PSS thin film below the surface were not affected by our solvent-structuring strategy.

To further analyze the electronic transport properties of the PEDOT:PSS-LT sample, we performed nanoscale-resolved infrared nano-FTIR spectroscopy (Fig. 4). Fig. 4a shows the topography and Fig. 4b the simultaneously obtained infrared near-field image, recorded with the nano-FTIR spectrometer tuned to a fixed reference mirror position, such that all wavelengths interfere constructively (white light position). Interestingly, we observed a strong contrast between the lower and upper phases, indicating that they had distinct infrared properties. For analyzing the different PEDOT:PSS-LT phases, we recorded nano-FTIR amplitude spectra on the upper and lower phase, as illustrated in the inset of Fig. 4c. We observed two well-defined features: (*i*) a strongly decreasing amplitude signal for both phases at higher frequencies and (*ii*) the same spectral behavior for both phases, but with a reduced amplitude signal on the upper phase (red curve) compared to the lower phase (black curve). Both spectra revealed free-carrier Drude response [58] as the amplitude decreased continuously and strongly for increasing frequencies. This result was particularly striking since the upper phase of PEDOT:PSS-LT showed no conductivity in our nano-electrical TUNA experiments (Fig. 2). However, the spectral variation was much smaller in the upper phase compared to the lower phase. This can be understood by considering that the top layer was thin enough (~30 nm) such that the near fields can probe the material located below it, as reported for other systems [83]. We confirmed this interpretation in Fig. 4d, by modeling nano-FTIR amplitude spectra with the finite dipole model (see Experimental Section), where the upper polymer phase was modelled as a dielectric layer of 30 nm thickness and permittivity ε_{upper} and the lower layer is modelled as a Drude metal of $\varepsilon_{lower} = \varepsilon_\infty[1-\nu_p^2/(\nu^2+i\nu\gamma_p)]$, where ν_p is the plasma frequency, γ_p the electronic damping factor, and ε_∞ the high-frequency permittivity. We can match model and experiment for $\nu_p = 2200\ cm^{-1}$, $\gamma_p = 4000\ cm^{-1}$ and $\varepsilon_\infty = \varepsilon_{upper} = 2$, corroborating that the PEDOT:PSS-LT sample comprises a dielectric upper phase and a conductive lower phase. Furthermore, we extrapolate a DC-conductivity $\sigma = 2\pi c\varepsilon_0\varepsilon_\infty\nu_p^2/\gamma_p = 40$ S/cm (c being the speed of light) from the nano-FTIR data, which was in line with the conductivity values found in our TUNA experiments above.

Previous literature results showed also that the fabrication of surface nanostructures on conducting polymers thin films resulted in distinct phases, each one presenting particular electrical properties. For

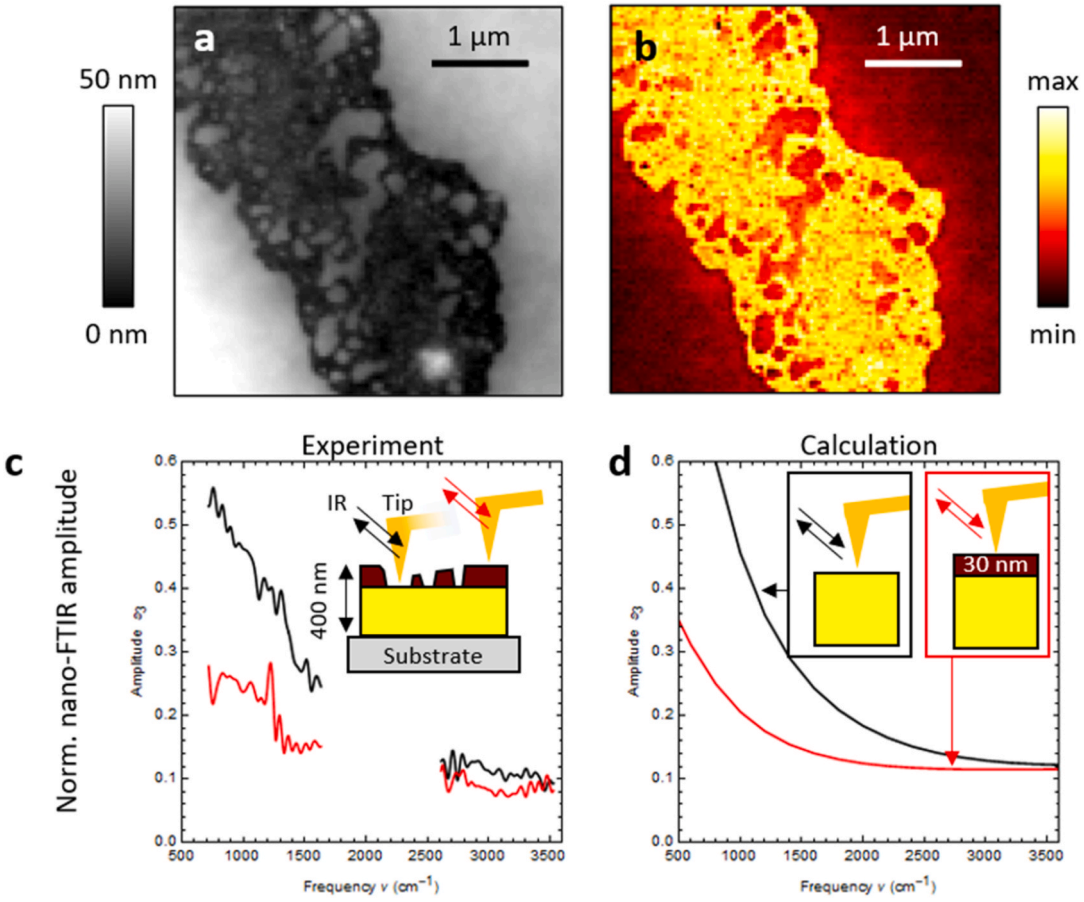

Fig. 4. nano-FTIR spectroscopy: (a) Topography and (b) infrared near-field image of the PEDOT:PSS-LT sample taken with mid-IR broadband radiation (υ = 700–1700 cm^{-1}) For imaging, the Fourier transform spectrometer is tuned to the white light position. (c) Experimental nano-FTIR amplitude spectra taken on the lower phase (black curve) and upper phase (red curve) of PEDOT:PSS-LT. Inset: Illustration of the sample and nano-FTIR spectroscopy on two different measurement spots. (d) Calculated nano-FTIR amplitude spectra of a conductive bulk material (black curve), and the same conductive material placed below a 30 nm-thick dielectric layer (red curve). (c,d) Spectra are normalized to a reference spectrum taken on silicon. (For interpretation of the references to color in this figure legend, the reader is referred to the Web version of this article.)

example, the preparation of laser-induced periodic surface structures on semiconducting polymers [84–86], as well as on PEDOT:PSS [27] resulted in the segregation of conducting regions, as evaluated by C-AFM. In the latter case, Gutiérrez-Fernández et al. suggested that the heterogenous conductivity of laser-structured PEDOT:PSS films could be related to a different distribution of PEDOT and PSS phases after irradiation. Since the PEDOT:PSS material is heated by the laser pulses, the PEDOT and PSS coordination could break, thus leading to the formation of PEDOT-rich areas, with high conductivities, and PSS-rich areas with an insulating behavior [27]. In our current work, the zero conductivity of the upper phase of the PEDOT:PSS-LT sample, could be related to different possibilities based on the rearrangement of the PEDOT and PSS phases due to solvent exposure. First, as already discussed, the non-conducting phase could be related to a vertical PEDOT/PSS phase separation. Under this idea, a *pure* PSS layer on the top of the PEDOT:PSS-LT film would result in a "dielectric spacer", hindering electronic transport. Second, instead of being a *pure* PSS layer, the upper phase could just be a PSS-rich layer where the PEDOT to PSS ratio is below the minimum required to allow the percolation of the conductive polymer grains into the electrolyte matrix, *i.e.*, 1 PEDOT unit for every 6 PSS chains for a Baytron P type [87]. In fact, the high conductivity of PEDOT:PSS is mostly related to its charge carriers density, which is governed by the PEDOT chains [88,89]. Then, as a third possibility, the non-conducting behavior of the PEDOT:PSS-LT upper phase could be related to a lower doping level onto the π-π conjugated system along the PEDOT chains, because of differences in the oxidation state of the PEDOT, from its polaron/bipolaron state to a neutral state [20–23].

3.3. Chemical identification of PEDOT/PSS phases in nanostructured PEDOT:PSS thin films

To further understand the chemical nature of the PEDOT:PSS-LT phases, we performed new experiments. Fig. 5 shows compound topography/electrical maps for PEDOT:PSS-LT samples, after washing using distilled water. On one hand, Fig. 5a shows the results after spin casting a drop of water onto a PEDOT:PSS-LT sample. On the other hand, Fig. 5b shows the results after immersing a PEDOT:PSS-LT film onto a water reservoir, at room temperature, for 10 s. We tested these ideas by following the work of DeLongchamp and collaborators, who observed that these protocols would allow removing PSS-rich areas, with negligible PEDOT loss [90]. As presented in Fig. 5, our AFM studies showed that no morphological or electrical changes took place after either treatment. This important result indicated that the upper layer of PEDOT:PSS-LT should not be composed by *free* PSS chains exclusively.

These facts were furthermore supported by a nanomechanical investigation of PEDOT:PSS-LT. Fig. 6 shows compound topography/mechanical modulus maps for pristine PEDOT:PSS (Fig. 6a) and PEDOT:PSS-LT (Fig. 6b). The pink areas in these maps denote zones where the Young's modulus values were above 2.7 GPa, as calculated from eqn (1). This modulus cutoff allowed identifying areas richer in PSS, as previously reported for pristine PEDOT:PSS thin films [50,91]. The original images used to create these maps are presented in Fig. S5. From Fig. 6a, we observed a homogeneous PSS distribution throughout the pristine thin film, as expected. However, the PEDOT:PSS-LT sample showed a distinctive nanomechanical phase separation. In particular, E_Y values above the threshold, indicating PSS presence, were preferentially located at the bottom phase of the film with a disposition comparable in shape and density as in the pristine case. On the contrary, the upper phase was mostly characterized by a slightly lower E_Y, which would be indicative of PEDOT-rich areas, as reported before [50].

Our nanoscale studies pointed out that the upper phase of PEDOT:PSS-LT must be rich in PEDOT chains. However, considering its low conducting properties, the surface chains should be composed by neutral PEDOT chains ($PEDOT^0$). On the contrary, the nanoscale properties of bottom phase remained fairly similar to those of a pristine PEDOT:PSS thin film. This latter fact indicated that at the conducting areas of PEDOT:PSS-LT, the PEDOT chains remained in the doped polar/bipolaron state ($PEDOT^{+/2+}$), stabilized by the presence of PSS counterions [92]. In other words, our results show that exposure of PEDOT:PSS to THF resulted in an enhanced mobility of polymer chains that allowed a vertical segregation from the granular PEDOT:PSS state in the volume of the thin film, in such a way a $PEDOT^0$ sheet was formed on top of the samples. A vertical phase separation of PEDOT and PSS phases has been observed by Yeo and collaborators [69], as discussed in section 3.2. However, in our current work, the use a low boiling point solvent favored PEDOT vertical segregation, instead of the PSS segregation observed previously when using DMSO [69]. The presence of a $PEDOT^0$ layer at the top of the nanostructured thin films can be interesting for potential applications of the material, for example for tuning its optoelectronic [11,93] and thermoelectric properties [22,23]. This is related to the fact that a $PEDOT^0$ sheet would allow to modify its surficial work function and hole transport properties by decreasing the charge carrier concentration at the interphase [82]. Finally, we point out that our strategy allowed a fast fabrication of nanostructured surface domains on PEDOT:PSS thin films, just by a controlled solvent exposure. This result opens the possibility of developing further solvent-based fabrication strategies able to tailor the structure and properties of PEDOT:PSS.

4. Conclusions

Solvent-structured PEDOT:PSS thin films were fabricated by exposing the material to controlled THF vapors. Spin casting THF onto the polymer thin films allowed a first approach into nanostructure fabrication. However, the method proved to be not reliable to ensure

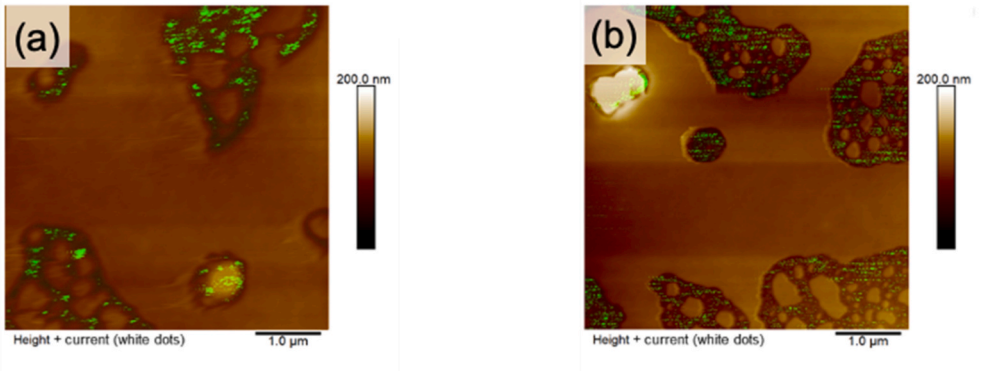

Fig. 5. Compound topography/electrical maps of PEDOT:PSS-LT film after (a) spin casting a H_2O drop, and (b) immersion into a H_2O bath. On both images, green shading indicates regions with current detection above 100 pA. (For interpretation of the references to color in this figure legend, the reader is referred to the Web version of this article.)

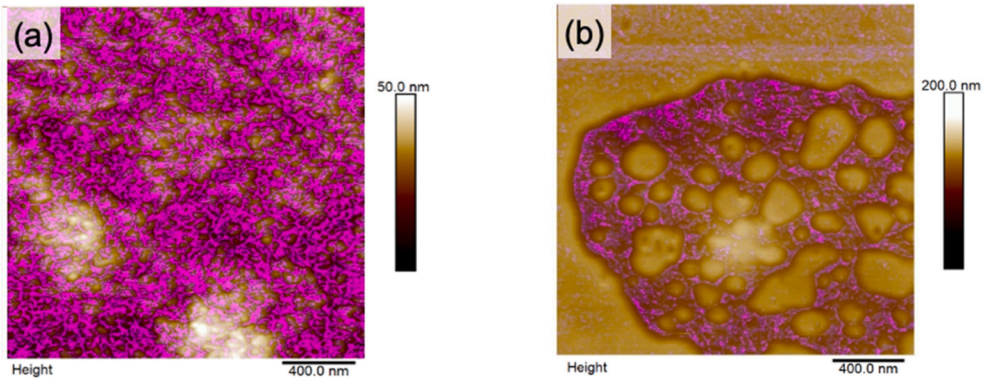

Fig. 6. Nanomechanical results, as compound topography/modulus maps, for pristine (a) PEDOT:PSS, and (b) PEDOT:PSS-LT. Pink shading refer to zones on the sample were the Young's modulus values were higher than 2.7 GPa. (For interpretation of the references to color in this figure legend, the reader is referred to the Web version of this article.)

homogeneity and good reproducibility. On the contrary, subjecting the films to a saturated THF atmosphere, by SVA, allowed the fabrication of controlled nanostructured PEDOT:PSS surfaces. The obtained samples showed distinct conducting areas at its upmost surface, while leaving unchanged the nanoelectrical properties of the volume. A combination of nanoscale methods allowed to determine that the exposure of PEDOT:PSS to THF vapors resulted in a vertical phase separation of the PEDOT and PSS components. In particular, we proved that the PEDOT chains moved preferentially towards the material surface, forming a discontinuous covering sheet. This surficial film, of 30 nm in thickness, was preferentially composed by neutral state surface PEDOT chains. This would allow to modify the surface work function and hole transport properties, opening the possibility of new applications of nanostructured PEDOT:PSS as optoelectronic and thermoelectric material.

CRediT authorship contribution statement

Matteo Sanviti: Conceptualization, Investigation, Writing – original draft. **Lars Mester:** Investigation, Writing – original draft. **Rainer Hillenbrand:** Writing – review & editing. **Angel Alegría:** Supervision, Project administration, Writing – review & editing. **Daniel E. Martínez-Tong:** Methodology, Project administration, Writing – review & editing.

Declaration of competing interest

The authors declare that they have no known competing financial interests or personal relationships that could have appeared to influence the work reported in this paper.

Acknowledgments

M. S., A. A. and D. E. M-T, acknowledge funding from the Basque Government (projects codes: IT-1175-19 and IT-1566-22) and the Spanish Ministry of Science and Innovation (*MCIU/AEI/FEDER; EU. Code: PID2019-104650GB-C21)*. R. H. and L. M., acknowledge funding from the Spanish Ministry of Science and Innovation (projects codes: RTI2018-094830-B-100 and MDM-2016-0618 of the Maria de Maeztu Units of Excellence Program) and from the Basque Government (projects codes: IT1164-19).

Appendix A. Supplementary data

Supplementary data to this article can be found online at https://doi.org/10.1016/j.polymer.2022.124723.

References

[1] X. Fan, W. Nie, H. Tsai, N. Wang, H. Huang, Y. Cheng, R. Wen, L. Ma, F. Yan, Y. Xia, PEDOT:PSS for flexible and stretchable electronics: modifications, strategies, and applications, Adv. Sci. 6 (2019), https://doi.org/10.1002/advs.201900813.
[2] Z. Fan, J. Ouyang, Thermoelectric properties of PEDOT:PSS, Adv. Electron. Mater. 5 (2019) 1–23, https://doi.org/10.1002/aelm.201800769.
[3] Y. Xu, Z. Liu, X. Wei, J. Wu, J. Guo, B. Zhao, H. Wang, S. Chen, Y. Dou, Morphological modulation to improve thermoelectric performances of PEDOT:PSS films by DMSO vapor post-treatment, Synth. Met. 271 (2021), 116628, https://doi.org/10.1016/j.synthmet.2020.116628.
[4] H.T. Cai, H. Xu, C. Tang, J. Li, Z.Y. Yang, S.H. Ye, W. Huang, Intrinsic ambipolar transport for the traditional conducting or hole transport ionic blend polymer PEDOT:PSS, Polymer 180 (2019), 121732, https://doi.org/10.1016/j.polymer.2019.121732.
[5] H. Song, Y. Yao, C. Tang, L. Zhang, Y. Lu, Q. Sun, F. Huang, C. Zuo, Tunable thermoelectric properties of free-standing PEDOT nanofiber film through adjusting its nanostructure, Synth. Met. 275 (2021), 116742, https://doi.org/10.1016/j.synthmet.2021.116742.
[6] N. Chaudhary, A. Singh, D.K. Aswal, M. Bharti, A. Sharma, A.R. Tillu, M. Roy, B. P. Singh, J. Bahadur, V. Putta, A.K. Debnath, High energy electron beam induced improved thermoelectric properties of PEDOT:PSS films, Polymer 202 (2020), 122645, https://doi.org/10.1016/j.polymer.2020.122645.
[7] S. Panigrahy, B. Kandasubramanian, Polymeric thermoelectric PEDOT: PSS & composites: synthesis, progress, and applications, Eur. Polym. J. 132 (2020), https://doi.org/10.1016/j.eurpolymj.2020.109726.
[8] Z. Sun, M. Shu, W. Li, P. Li, Y. Zhang, H. Yao, S. Guan, Enhanced thermoelectric performance of PEDOT:PSS self-supporting thick films through a binary treatment with polyethylene glycol and water, Polymer 192 (2020), 122328, https://doi.org/10.1016/j.polymer.2020.122328.
[9] A.C. Hinckley, S.C. Andrews, M.T. Dunham, A. Sood, M.T. Barako, S. Schneider, M. F. Toney, K.E. Goodson, Z. Bao, Achieving high thermoelectric performance and metallic transport in solvent-sheared PEDOT:PSS, Adv. Electron. Mater. 7 (2021) 1–9, https://doi.org/10.1002/aelm.202001190.
[10] E. Vitoratos, S. Sakkopoulos, N. Poliatsas, K. Emmanouil, S.A. Choulis, Conductivity degradation study of PEDOT: PSS films under heat treatment in helium and atmospheric air, Open J. Org. Polym. Mater. (2012) 7–11, https://doi.org/10.4236/ojopm.2012.21004, 02.
[11] Z. Wang, L. Gao, X. Wei, M. Zhao, Y. Miao, X. Zhang, H. Zhang, H. Wang, Y. Hao, B. Xu, J. Guo, Energy level engineering of PEDOT:PSS by antimonene quantum sheet doping for highly efficient OLEDs, J. Mater. Chem. C. 8 (2020) 1796, https://doi.org/10.1039/c9tc06049a.
[12] C.C. Lo, S. Sudheendran Swayamprabha, T.C. Hsueh, S.D. Chavhan, R.A.K. Yadav, J.R. Lee, K.K. Kesavan, S.Z. Chen, C.W. Wang, J.H. Jou, Modification effect of hole injection layer on efficiency performance of wet-processed blue organic light emitting diodes, Org. Electron. 92 (2021), 106084, https://doi.org/10.1016/j.orgel.2021.106084.
[13] K.M. Reza, A. Gurung, B. Bahrami, S. Mabrouk, H. Elbohy, R. Pathak, K. Chen, A. H. Chowdhury, M.T. Rahman, S. Letourneau, H.C. Yang, G. Saianand, J.W. Elam, S. B. Darling, Q. Qiao, Tailored PEDOT:PSS hole transport layer for higher performance in perovskite solar cells: enhancement of electrical and optical properties with improved morphology, J. Energy Chem. 44 (2020) 41–50, https://doi.org/10.1016/j.jechem.2019.09.014.
[14] W. Han, G. Ren, J. Liu, Z. Li, H. Bao, C. Liu, W. Guo, Recent progress of inverted perovskite solar cells with a modified PEDOT:PSS hole transport layer, ACS Appl. Mater. Interfaces 12 (2020), 49322, https://doi.org/10.1021/acsami.0c13576.
[15] S.H. Chang, C.C. Chen, H.M. Cheng, S.H. Chen, Structural, optical, electrical and electronic properties of PEDOT: PSS thin films and their application in solar cells, Printable Sol. Cells (2017) 263–288, https://doi.org/10.1002/9781119283720.ch8.

[16] H. Shi, C. Liu, Q. Jiang, J. Xu, Effective approaches to improve the electrical conductivity of PEDOT:PSS: a review, Adv. Electron. Mater. 1 (2015) 1–16, https://doi.org/10.1002/aelm.201500017.
[17] Z. Zhao, G.F. Richardson, Q. Meng, Effect of liquid immersion of PEDOT: PSS-coated polyester fabric on surface resistance and wettability, Smart Mater. Struct. 26 (2017), 065016, https://doi.org/10.1088/1361-665X/aa6f25.
[18] S.H. Lee, J.S. Sohn, S.B. Kulkarni, U.M. Patil, S.C. Jun, J.H. Kim, Modified physico-chemical properties and supercapacitive performance via DMSO inducement to PEDOT:PSS active layer, Org. Electron. 15 (2014) 3423–3430, https://doi.org/10.1016/j.orgel.2014.09.020.
[19] A. Fallahzadeh, J. Saghaei, M.H. Yousefi, Effect of alcohol vapor treatment on electrical and optical properties of poly(3,4-ethylene dioxythiophene):poly(styrene sulfonate) films for indium tin oxide-free organic light-emitting diodes, Appl. Surf. Sci. 320 (2014) 895–900, https://doi.org/10.1016/j.apsusc.2014.09.143.
[20] F.L.E. Jakobsson, X. Crispin, L. Lindell, A. Kanciurzewska, M. Fahlman, W. R. Salaneck, M. Berggren, Towards all-plastic flexible light emitting diodes, Chem. Phys. Lett. 433 (2006) 110–114, https://doi.org/10.1016/j.cplett.2006.11.007.
[21] M. Reyes-Reyes, R. López-Sandoval, E. Tovar-Martínez, J.V. Cabrera-Salazar, G. Martínez-Ponce, Tuning the dedoping process of PEDOT:PSS films using DBU-solvent complexes, Synth. Met. 243 (2018) 25–33, https://doi.org/10.1016/j.synthmet.2018.05.004.
[22] Q. Li, Q. Zhou, L. Wen, W. Liu, Enhanced thermoelectric performances of flexible PEDOT:PSS film by synergistically tuning the ordering structure and oxidation state, J. Mater. 6 (2020) 119–127, https://doi.org/10.1016/j.jmat.2020.01.001.
[23] T.C. Tsai, H.C. Chang, C.H. Chen, Y.C. Huang, W.T. Whang, A facile dedoping approach for effectively tuning thermoelectricity and acidity of PEDOT:PSS films, Org. Electron. 15 (2014) 641–645, https://doi.org/10.1016/j.orgel.2013.12.023.
[24] X. Hu, G. Chen, X. Wang, H. Wang, Tuning thermoelectric performance by nanostructure evolution of a conducting polymer, J. Mater. Chem. (2015) 20896–20902, https://doi.org/10.1039/c5ta07381b.
[25] A. Radivo, A. Enrico Sovernigo, A. Marco Caputo, S. Dal Zilio, T. Endale, A. Pozzato, A. Goldoni, M. Tormen, Patterning PEDOT:PSS and tailoring its electronic properties by water-vapour-assisted nanoimprint lithography, RSC Adv. 4 (2014) 34014–34025, https://doi.org/10.1039/c4ra04807e.
[26] E. Gutiérrez-Fernández, I.A. Gabaldón-Saucedo, M.C. García-Gutiérrez, A. Varea, A. Nogales, E. Rebollar, A. Vilà, T.A. Ezquerra, A. Cirera, Quantitative assessment by local probe methods of the mechanical and electrical properties of inkjet-printed PEDOT:PSS thin films over Indium Tin Oxide substrates, Org. Electron. 70 (2019) 258–263, https://doi.org/10.1016/j.orgel.2019.04.020.
[27] E. Gutiérrez-Fernández, I.A. Gabaldón-Saucedo, Á. Rodríguez-Rodríguez, E. Solano, M.C. García-Gutiérrez, A. Nogales, A. Cirera, T.A. Ezquerra, E. Rebollar, Laser nanostructuring of thin films of PEDOT:PSS on ITO: morphology, molecular structure and electrical properties, Appl. Surf. Sci. 509 (2020), https://doi.org/10.1016/j.apsusc.2020.145350.
[28] S.F. Tseng, W.T. Hsiao, K.C. Huang, D. Chiang, Electrode patterning on PEDOT:PSS thin films by pulsed ultraviolet laser for touch panel screens, Appl. Phys. Mater. Sci. Process 112 (2013) 41–47, https://doi.org/10.1007/s00339-012-7172-3.
[29] J.H. Choi, H.J. Choi, J.H. Shin, H.P. Kim, J. Jang, H. Lee, Enhancement of organic solar cell efficiency by patterning the PEDOT:PSS hole transport layer using nanoimprint lithography, Org. Electron. 14 (2013) 3180–3185, https://doi.org/10.1016/j.orgel.2013.09.020.
[30] F.-C. Tang, F.-C. Wu, C.-T. Yen, J. Chang, W.-Y. Chou, S.-H.G. Chang, H.-L. Cheng, A nanoscale study of charge extraction in organic solar cells: the impact of interfacial molecular configuration, Nanoscale 7 (2014) 104, https://doi.org/10.1039/c4nr03176h.
[31] E. Moyen, A. Hama, E. Ismailova, L. Assaud, G.G. Malliaras, M. Hanbuken, R. M. Owens, Nanostructured conducting polymers for stiffness controlled cell adhesion, Nanotechnology 27 (2016), 074001, https://doi.org/10.1088/0957-4484/27/7/074001.
[32] M. Mirsafaei, A. Hossein Fallahpour, P. Lugli, H.-G. Rubahn, J. Adam, M. Madsen, The influence of electrical effects on device performance of organic solar cells with nano-structured electrodes, Sci. Rep. 7 (2017) 5300, https://doi.org/10.1038/s41598-017-05591-8.
[33] D. Ohayon, C. Pitsalidis, A.-M. Pappa, A. Hama, Y. Zhang, L. Gallais, R.M. Owens, Laser patterning of self-assembled monolayers on PEDOT:PSS films for controlled cell adhesion, Adv. Mater. Interfac. 4 (2017), 1700191, https://doi.org/10.1002/admi.201700191.
[34] J. Li, X. Chang, S. Li, K. Shrestha, E.K.W. Tan, D. Chu, High-resolution electrochemical transistors defined by mold-guided drying of PEDOT:PSS liquid suspension, ACS Appl. Electron. Mater. 2 (2020) 2611–2618, https://doi.org/10.1021/acsaelm.0c00491.
[35] A.F. Lasagni, J.L. Hendricks, C.M. Shaw, D. Yuan, D.C. Martin, S. Das, Direct laser interference patterning of poly(3,4-ethylene dioxythiophene)-poly(styrene sulfonate) (PEDOT-PSS) thin films, Appl. Surf. Sci. 255 (2009) 9186–9192, https://doi.org/10.1016/j.apsusc.2009.06.130.
[36] D. Yuan, A. Lasagni, J.L. Hendricks, D.C. Martin, S. Das, Patterning of periodic nano-cavities on PEDOT-PSS using nanosphere-assisted near-field optical enhancement and laser interference lithography Related content, Nanotechnology 23 (2012), 015304, https://doi.org/10.1088/0957-4484/23/1/015304.
[37] J.Y. Li, H. Yu, J.J. Wen, Z.D. Li, Z.C. Xu, Y.F. Zhang, H. Yu, B.R. Lu, R. Liu, Y. F. Chen, Fabrication of nano-strctures on PEDOT:PSS film by nanoimprint lithography, Adv. Mater. Res. 465 (2012) 287–291. https://doi.org/10.4028/www.scientific.net/AMR.465.287.
[38] A. - D.A. Rider, R.T. Tucker, B.J. Worfolk, Y.-S. Hsiao, W.-T. Whang, S.-C. Suen, H. Park, J.A. Rowehl, K. Kang Kim, M. Jong Han, Y. Yang, K. Lee, K. Mielczarek, W. Hu, A. Zakhidov, Nanoimprint of dehydrated PEDOT:PSS for organic photovoltaics, Nanotechnology 22 (2011) 485301–485306, https://doi.org/10.1088/0957-4484/22/48/485301.
[39] M. Elmahmoudy, A.M. Charrier, G.G. Malliaras, S. Sanaur, Facile nanopatterning of PEDOT:PSS thin films, Adv. Mater. Technol. 3 (2018), 1700344, https://doi.org/10.1002/admt.201700344.
[40] H. Sun, Recent Progress in Low Temperature Nanoimprint Lithography, vol. 21, 2015, pp. 1–7, https://doi.org/10.1007/s00542-014-2366-6.
[41] D. Schaubroeck, J. De Smet, W. Willems, P. Cools, N. De Geyter, R. Morent, H. De Smet, G. Van Steenbeerge, Surface analysis of the selective excimer laser patterning of a thin PEDOT:PSS film on flexible polymer films, Appl. Surf. Sci. 376 (2016) 151–160, https://doi.org/10.1016/j.apsusc.2016.03.125.
[42] D.E. Martínez-Tong, C. Ruzie, Y.H. Geerts, M. Sferrazza, Structural evolution of an organic semiconducting molecule onto a soft substrate, ChemPhysChem 17 (2016) 1174–1179, https://doi.org/10.1002/cphc.201501144, 2016.
[43] L.S.C. Pingree, O.G. Reid, D.S. Ginger, Electrical scanning probe microscopy on active organic electronic devices, Adv. Mater. 21 (2009) 19–28, https://doi.org/10.1002/adma.200801466.
[44] J.E. Sader, J.W.M. Chon, P. Mulvaney, Calibration of rectangular atomic force microscope cantilevers, Rev. Sci. Instrum. 70 (1999) 3967, https://doi.org/10.1063/1.1150021.
[45] J.E. Sader, R. Borgani, C.T. Gibson, D.B. Haviland, M.J. Higgins, J.I. Kilpatrick, J. Lu, P. Mulvaney, C.J. Shearer, A.D. Slattery, A. Thorén, J. Tran, H. Zhang, H. Zhang, T. Zheng, A Virtual Instrument to Standardise the Calibration of Atomic Force Microscope Cantilevers, 2016, https://doi.org/10.1063/1.4962866.
[46] H.J. Lee, J. Lee, S.M. Park, Electrochemistry of conductive polymers. 45. Nanoscale conductivity of PEDOT and PEDOT:PSS composite films studied by current-sensing AFM, J. Phys. Chem. B 114 (2010) 2660–2666, https://doi.org/10.1021/jp9113859.
[47] B. Cappella, G. Dietler, Force-distance curves by atomic force microscopy, Surf. Sci. Rep. 34 (1999) 1–3, https://doi.org/10.1016/S0167-5729(99)00003-5.
[48] G. Stan, R.S. Gates, M.R. Rosenberger, S. Chen, C.B. Prater, The use of the PeakForce TM quantitative nanomechanical mapping AFM-based method for high-resolution Young's modulus measurement of polymers, Meas. Sci. Technol. 22 (2011), 125703, https://doi.org/10.1088/0957-0233/22/12/125703.
[49] O. Sahin, N. Erina, R. Wagner, R. Moon, J. Pratt, G. Shaw, A. Raman, Uncertainty quantification in nanomechanical measurements using the atomic force microscope, Nanotechnology 22 (2011) 455703–455712, https://doi.org/10.1088/0957-4484/22/45/455703.
[50] M. Sanviti, A. Alegria, D.E. Martínez-Tong, Fabrication and nanoscale properties of PEDOT:PSS conducting polymer nanospheres, ChemRxiv (2021) 1–29, https://doi.org/10.26434/chemrxiv.14135315.
[51] K. Xu, W. Sun, Y. Shao, F. Wei, X. Zhang, W. Wang, P. Li, Recent development of PeakForce Tapping mode atomic force microscopy and its applications on nanoscience, Nanotechnol. Rev. 7 (2018) 605–621, https://doi.org/10.1515/ntrev-2018-0086.
[52] S. Zhang, Y. Weng, C. Ma, Quantitative nanomechanical mapping of polyolefin elastomer at nanoscale with atomic force microscopy, Nanoscale Res. Lett. 16 (2021) 113, https://doi.org/10.1186/s11671-021-03568-1.
[53] V.M. Muller, B.V. Derjaguin, Y.P. Toporov, On two methods of calculation of the force of sticking of an elastic sphere to a rigid plane, Colloid. Surface. 7 (1983) 251–259, https://doi.org/10.1016/0166-6622(83)80051-1.
[54] S. Fujinami, E. Ueda, K. Nakajima, T. Nishi, Analytical methods to derive the elastic modulus of soft and adhesive materials from atomic force microcopy force measurements, J. Polym. Sci., Part B: Polym. Phys. 57 (2019) 1279–1286, https://doi.org/10.1002/polb.24871.
[55] F. Huth, A. Govyadinov, S. Amarie, W. Nuansing, F. Keilmann, R. Hillenbrand, Nano-FTIR absorption spectroscopy of molecular fingerprints at 20 nm spatial resolution, Nano Lett. 12 (2012) 3973–3978, https://doi.org/10.1021/nl301159v.
[56] F. Huth, M. Schnell, J. Wittborn, N. Ocelic, R. Hillenbrand, Infrared-spectroscopic nanoimaging with a thermal source, Nat. Mater. 10 (2011) 352–356, https://doi.org/10.1038/nmat3006.
[57] X. Chen, D. Hu, R. Mescall, G. You, D.N. Basov, Q. Dai, M. Liu, Modern scattering-type scanning near-field optical microscopy for advanced material research, Adv. Mater. 31 (2019) 1–24, https://doi.org/10.1002/adma.201804774.
[58] F. Keilmann, A.J. Huber, R. Hillenbrand, Nanoscale conductivity contrast by scattering-type near-field optical microscopy in the visible, infrared and THz domains, J. Infrared, Millim. Terahertz Waves 30 (2009) 1255–1268, https://doi.org/10.1007/s10762-009-9525-3.
[59] L. Novotny, B. Hecht, Principles of Nano-Optics, Cambridge University Press, Cambridge, 2012, https://doi.org/10.1017/CBO9780511794193.
[60] A. Cvitkovic, N. Ocelic, R. Hillenbrand, Analytical model for quantitative prediction of material contrasts in scattering-type near-field optical microscopy, Opt Express 15 (2007) 8550, https://doi.org/10.1364/oe.15.008550.
[61] B. Hauer, A.P. Engelhardt, T. Taubner, Quasi-analytical model for scattering infrared near-field microscopy on layered systems, Opt Express 20 (2012), 13173, https://doi.org/10.1364/oe.20.013173.
[62] H. Cho, W. Cho, Y. Kim, J.G. Lee, J.H. Kim, Influence of residual sodium ions on the structure and properties of poly(3,4-ethylenedioxythiophene):poly (styrenesulfonate), RSC Adv. 8 (2018) 29044–29050, https://doi.org/10.1039/c8ra05150j.
[63] H. Yan, H. Okuzaki, Effect of solvent on PEDOT/PSS nanometer-scaled thin films: XPS and STEM/AFM studies, Synth. Met. 159 (2009) 2225–2228, https://doi.org/10.1016/j.synthmet.2009.07.032.
[64] A. Pasha, S. Khasim, O.A. Al-Hartomy, M. Lakshmi, K.G. Manjunatha, Highly sensitive ethylene glycol-doped PEDOT-PSS organic thin films for LPG sensing, RSC Adv. 8 (2018) 18074–18083, https://doi.org/10.1039/c8ra01061g.

[65] U. Lang, E. Müller, N. Naujoks, J. Dual, Microscopical investigations of PEDOT:PSS thin films, Adv. Funct. Mater. 19 (2009) 1215–1220, https://doi.org/10.1002/adfm.200801258.
[66] T. Horii, H. Hikawa, M. Katsunuma, H. Okuzaki, Synthesis of highly conductive PEDOT:PSS and correlation with hierarchical structure, Polymer 140 (2018) 33–38, https://doi.org/10.1016/j.polymer.2018.02.034.
[67] Q. Niu, W. Huang, J. Tong, H. Lv, Y. Deng, Y. Ma, Z. Zhao, R. Xia, W. Zeng, Y. Min, W. Huang, Understanding the mechanism of PEDOT: PSS modification via solvent on the morphology of perovskite films for efficient solar cells, Synth. Met. 243 (2018) 17–24, https://doi.org/10.1016/j.synthmet.2018.05.012.
[68] M. Girtan, R. Mallet, M. Socol, A. Stanculescu, On the physical properties PEDOT: PSS thin films, Mater. Today Commun. 22 (2020), 100735, https://doi.org/10.1016/j.mtcomm.2019.100735.
[69] J.-S. Yeo, J.-M. Yun, D.-Y. Kim, S. Park, S.-S. Kim, M.-H. Yoon, T.-W. Kim, S.-I. Na, Significant vertical phase separation in solvent-vapor-annealed poly(3,4-ethylenedioxythiophene):poly(styrene sulfonate) composite films leading to better conductivity and work function for high-performance indium tin oxide-free optoelectronics, ACS Appl. Mater. Interfaces 4 (2012) 2551–2560, https://doi.org/10.1021/am300231v.
[70] H. Liu, X. Li, L. Zhang, Q. Hong, J. Tang, A. Zhang, C.Q. Ma, Influence of the surface treatment of PEDOT:PSS layer with high boiling point solvent on the performance of inverted planar perovskite solar cells, Org. Electron. 47 (2017) 220–227, https://doi.org/10.1016/j.orgel.2017.05.025.
[71] S.P. Rwei, Y.H. Lee, J.W. Shiu, R. Sasikumar, U.T. Shyr, Characterization of solvent-treated PEDOT:PSS thin films with enhanced conductivities, Polymers 11 (2019), https://doi.org/10.3390/polym11010134.
[72] X.-Y. Li, L.-P. Zhang, F. Tang, Z.-M. Bao, J. Lin, Y.-Q. Li, L. Chen, C.-Q. Ma, The solvent treatment effect of the PEDOT:PSS anode interlayer in inverted planar perovskite solar cells, RSC Adv. 6 (2016) 24501–24507, https://doi.org/10.1039/c5ra25787e.
[73] R. Misael Vedovatte, Matheus C. Saccardo, Eduardo Lima Costa, C.E. Cava, PEDOT: PSS post-treated by DMSO using spin coating, roll-to-roll and immersion: a comparative study, J. Mater. Sci. Mater. Electron. 31 (2020) 317–323, https://doi.org/10.1007/s10854-019-02524-1.
[74] Q. Jiang, C. Liu, H. Song, H. Shi, Y. Yao, J. Xu, G. Zhang, B. Lu, Improved thermoelectric performance of PEDOT:PSS films prepared by polar-solvent vapor annealing method, J. Mater. Sci. Mater. Electron. 24 (2013) 4240–4246, https://doi.org/10.1007/s10854-013-1391-z.
[75] J.S. Yeo, J.M. Yun, D.Y. Kim, S.S. Kim, S.I. Na, Successive solvent-treated PEDOT: PSS electrodes for flexible ITO-free organic photovoltaics, Sol. Energy Mater. Sol. Cells 114 (2013) 104–109, https://doi.org/10.1016/j.solmat.2013.02.031.
[76] L.V. Lingstedt, M. Ghittorelli, H. Lu, D.A. Koutsouras, T. Marszalek, F. Torricelli, N. I. Cra, P. Gkoupidenis, P.W.M. Blom, Effect of DMSO solvent treatments on the performance of PEDOT:PSS based organic electrochemical transistors, Adv. Electron. Mater. 5 (2019), 1800804, https://doi.org/10.1002/aelm.201800804.
[77] X. Wang, P. Liu, Q. Jiang, W. Zhou, J. Xu, J. Liu, Y. Jia, X. Duan, Y. Liu, Y. Du, F. Jiang, Efficient DMSO-vapor annealing for enhancing thermoelectric performance of PEDOT:PSS-based aerogel, ACS Appl. Mater. Interfaces 11 (2019) 2408–2417, https://doi.org/10.1021/acsami.8b19168.
[78] G. Liu, X. Xie, Z. Liu, G. Cheng, E.-C. Lee, Alcohol based vapor annealing of a poly (3,4-ethylenedioxythiophene):poly(styrenesulfonate) layer for performance improvement of inverted perovskite solar cells, Nanoscale 10 (2018), 11043, https://doi.org/10.1039/c8nr02146e.
[79] V. Castagnola, C. Bayon, E. Descamps, C. Bergaud, Morphology and conductivity of PEDOT layers produced by different electrochemical routes, Synth. Met. 189 (2014) 7–16, https://doi.org/10.1016/j.synthmet.2013.12.013.
[80] L.S.C. Pingree, B.A. Macleod, D.S. Ginger, The changing face of PEDOT:PSS films: substrate, bias, and processing effects on vertical charge transport, J. Phys. Chem. C 112 (2008) 7922–7927, https://doi.org/10.1021/jp711838h.
[81] J.M. Mativetsky, J. Tarver, X. Yang, B.E. Koel, Y.L. Loo, Structural origin of anisotropic transport in electrically conducting dichloroacetic acid-treated polymers, Org. Electron. 15 (2014) 631–638, https://doi.org/10.1016/j.orgel.2013.12.019.
[82] N. Kim, I. Petsagkourakis, S. Chen, M. Berggren, X. Crispin, M.P. Jonsson, I. Zozoulenko, Electric Transport Properties in PEDOT Thin Films, 2019, https://doi.org/10.1201/9780429190520-3.
[83] L. Mester, A.A. Govyadinov, S. Chen, M. Goikoetxea, R. Hillenbrand, Subsurface chemical nanoidentification by nano-FTIR spectroscopy, Nat. Commun. 11 (2020) 1–10, https://doi.org/10.1038/s41467-020-17034-6.
[84] E. Gutiérrez-Fernández, Á. Rodríguez-Rodríguez, M.C. García-Gutiérrez, A. Nogales, T.A. Ezquerra, E. Rebollar, Functional nanostructured surfaces induced by laser on fullerene thin films, Appl. Surf. Sci. 476 (2019) 668–675, https://doi.org/10.1016/j.apsusc.2019.01.141.
[85] A. Rodríguez-Rodríguez, E. Rebollar, T.A. Ezquerra, M. Castillejo, J.V. Garcia-Ramos, M.-C. García-Gutiérrezgutiérrez, Patterning conjugated polymers by laser: synergy of nanostructure formation in the all-polymer heterojunction P3HT/PCDTBT, Langmuir 34 (2018) 115–125, https://doi.org/10.1021/acs.langmuir.7b03761.
[86] A. Rodríguez-Rodríguez, E. Rebollar, M. Soccio, T.A. Ezquerra, D.R. Rueda, J. Vicente Garcia-Ramos, M. Castillejo, M.-C. Garcia-Gutierrez, Laser-induced periodic surface structures on conjugated polymers: poly(3-hexylthiophene), Macromolecules 48 (2015) 4024–4031, https://doi.org/10.1021/acs.macromol.5b00804.
[87] T. Stoker, A. Kohler, R. Moos, Why does the electrical conductivity in PEDOT:PSS decrease with PSS content? A study combining thermoelectric measurements with impedance spectroscopy, J. Polym. Sci., Part B: Polym. Phys. 50 (2012) 976–983, https://doi.org/10.1002/polb.23089.
[88] L. Stepien, A. Roch, S. Schlaier, I. Dani, A. Kiriy, F. Simon, M.v. Lukowicz, C. Leyens, Investigation of the thermoelectric power factor of KOH-treated PEDOT: PSS dispersions for printing applications, Energy Harvest. Syst. 3 (2016) 101–111, https://doi.org/10.1515/ehs-2014-0060.
[89] L. Zhang, K. Yang, R. Chen, Y. Zhou, S. Chen, Y. Zheng, M. Li, C. Xu, X. Tang, Z. Zang, K. Sun, The role of mineral acid doping of PEDOT:PSS and its application in organic photovoltaics, Adv. Electron. Mater. 6 (2020), 1900648, https://doi.org/10.1002/aelm.201900648.
[90] D.M. DeLongchamp, B.D. Vogt, C.M. Brooks, K. Kano, J. Obrzut, C.A. Richter, O. A. Kirillov, E.K. Lin, Influence of a water rinse on the structure and properties of poly(3,4-ethylene dioxythiophene):Poly(styrene sulfonate) films, Langmuir 21 (2005) 11480–11483, https://doi.org/10.1021/la051403l.
[91] D. Tank, H.H. Lee, D.Y. Khang, Elastic moduli of organic electronic materials by the buckling method, Macromolecules 42 (2009) 7079–7083, https://doi.org/10.1021/ma900137k.
[92] M. Modarresi, A. Mehandzhiyski, M. Fahlman, K. Tybrandt, I. Zozoulenko, Microscopic understanding of the granular structure and the swelling of PEDOT: PSS, Macromolecules 53 (2020) 6267–6278, https://doi.org/10.1021/acs.macromol.0c00877.
[93] Z. Li, Y. Liang, Z. Zhong, J. Qian, G. Liang, K. Zhao, H. Shi, S. Zhong, Y. Yin, W. Tian, A low-work-function, high-conductivity PEDOT:PSS electrode for organic solar cells with a simple structure, Synth. Met. 210 (2015) 363–366, https://doi.org/10.1016/j.synthmet.2015.11.006.